Preprint typeset in JINST style - HYPER VERSION

arXiv:1311.1628v1 [physics.ins-det] 7 Nov 2013

Electrical Characterization of a Thin Edgeless N-on-p Planar Pixel Sensors For ATLAS Upgrades

---

Marco Bomben[1],[*] **Alvise Bagolini**[2], **Maurizio Boscardin**[2], **Luciano Bosisio**[3], **Giovanni Calderini**[1,4], **Jacques Chauveau**[1], **Gabriele Giacomini**[2], **Alessandro La Rosa**[5], **Giovanni Marchiori**[1] **and Nicola Zorzi**[2]

[1]*Laboratoire de Physique Nucleaire et de Hautes Énergies (LPNHE), Paris, France*
[2]*Fondazione Bruno Kessler, Centro per i Materiali e i Microsistemi (FBK-CMM), Povo di Trento (TN), Italy*
[3]*Università di Trieste, Dipartimento di Fisica and INFN, Trieste, Italy*
[4]*Dipartimento di Fisica E. Fermi, Università di Pisa, and INFN Sez. di Pisa, Pisa, Italy*
[5]*Section de Physique (DPNC), Universitè de Genève, Genève, Switzerland*
E-mail: `marco.bomben@lpnhe.in2p3.fr`

ABSTRACT: In view of the LHC upgrade phases towards the High Luminosity LHC (HL-LHC), the ATLAS experiment plans to upgrade the Inner Detector with an all-silicon system. Because of its radiation hardness and cost effectiveness, the n-on-p silicon technology is a promising candidate for a large area pixel detector. The paper reports on the joint development, by LPNHE and FBK of novel n-on-p edgeless planar pixel sensors, making use of the active trench concept for the reduction of the dead area at the periphery of the device. After discussing the sensor technology, and presenting some sensors' simulation results, a complete overview of the electrical characterization of the produced devices will be given.

KEYWORDS: Fabrication technology; TCAD simulations; Planar silicon radiation detectors; Slim edge Sensors.

---

[*] Corresponding author.

Contents

1. Introduction **1**

2. The active edge production **2**

3. TCAD simulations **2**

4. Performance evaluation **4**

5. Conclusions and outlook **7**

1. Introduction

The High Luminosity LHC (HL-LHC) will begin collisions around 2024 and will provide a leveled instantaneous luminosity of $5 \times 10^{34}\mathrm{cm}^{-2}\mathrm{s}^{-1}$, with the aim of delivering an additional 2500 fb^{-1} to ATLAS over ten years. By then the ATLAS experiment will be equipped with a completely new Pixel Detector . The innermost layer of the new pixel detector will integrate a fluence of about $10^{16}\,1\,\mathrm{MeV}\,\mathrm{n_{eq}}/\mathrm{cm}^2$ for an integrated luminosity of 3000 fb^{-1} ($\sim$ 10 years of operation). These harsh conditions demand radiation-hard devices and a finely segmented detector to cope with the expected high occupancy. The new pixel sensors will need to have high geometrical acceptance: the future material budget restrictions and tight mechanical constraints require the geometric inefficiency to be less than 2.5% [2]. One way to reduce or even eliminate the insensitive region along the device periphery is offered by the "active edge" technique [3], in which a deep vertical trench is etched along the device periphery throughout the entire wafer thickness, thus performing a damage free cut (this requires using a support wafer, to prevent the individual chips from getting loose). The trench is then heavily doped, extending the ohmic back-contact to the lateral sides of the device: the depletion region can then extend to the edge without causing a large current increase. This is the technology that was chosen bt FBK-Trento and LPNHE-Paris for realizing n-on-p pixel sensors with reduced inactive zone whose features and measurement results are reported in this paper.

The paper is organized as follows: in Section 2 the active edge technology chosen for a first production of n-on-p sensors is presented. Studies performed with TCAD simulation tools helped in defining the layout and making a first estimation of the charge collection efficiency expected after irradiation; they are presented in Section 3. In Section 4 the results from the electrical characterization of the sensors will be shown. Eventually, in Section 5 some conclusions will be drawn and future plans will be outlined.

name	# of GRs	pixel-to-trench distance (μm)
S1	0	100
S2	2	100
S3	1	100
S4	3	200
S5	3	200
S6	3	200
S7	3	200
S8	5	300
S9	10	400

Table 1. The list of the different FE-I4 compatible-sensor layouts. Two different designs are envisaged for the sensor with 3 GRs and 200 μm pixel-to-trench distance. See text for more details.

2. The active edge production

The sensors are fabricated on 100 mm diameter, high resistivity, p-type, Float Zone (FZ), <100> oriented, 200 μm thick wafers. The active edge technology is used, which is a single sided process, featuring a doped trench, extending all the way through the wafer thickness, and completely surrounding the sensor. For mechanical reasons, a support wafer is needed. Both homogeneous ("p-spray") and patterned ("p-stop") implants have been used to prevent pixels shorting due to the positive fixed charge present in the oxide. A boron implant for the ohmic contact to the substrate ("bias tab") is also added. More details on the adopted active edge technique and on the production in general can be found in [4]. Nine FE-I4 readout chip [5] compatible pixel sensors were put on each wafer; each sensor consists of an array of 336 × 80 pixels, at a pitch of 50 μm × 250 μm, for an overall sensitive area of 16.8 mm × 20.0 mm. The nine FE-I4 sensors differ in the pixel-to-trench distance (100, 200, 300, and 400 μm) and in the number of the guard rings (0, 1, 2, 3, 5, and 10) surrounding the pixel area. The sensor with 3 GRs and a 200 μm pixel-to-trench distance features two different GR designs, and each of them is repeated twice. A list of the different FE-I4 sensor versions is reported in Table 1.

3. TCAD simulations

In order to explore and compare the properties of the design variations considered, numerical simulations were performed with TCAD tools from SILVACO [6]. 2D structures have been simulated, varying parameters like the number of GRs and the pixel-to-trench distance. Among all the observables that could be studied, the charge collection efficiency (CCE), for simulated un-irradiated and irradiated sensors, was the more interesting. To describe the radiation damage, an effective model based on three deep levels in the forbidden gap was used [7]. Radiation-induced interface traps at the Si-SiO$_2$ interface are also included in the simulation, as described in [8].

To study charge collection efficiency (CCE) after irradiation, charge creation in irradiated sensors was simulated. The most interesting case is when the charge is released in the gap between the pixel and the trench, when no GRs are present. If a significant amount of charge can be collected

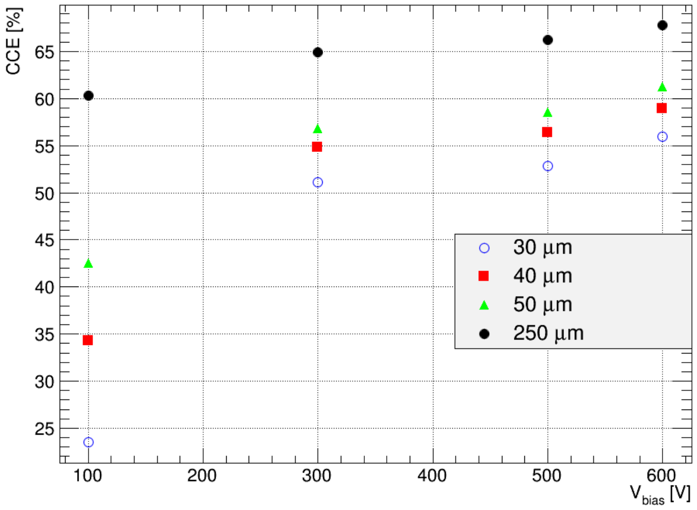

Figure 1. Charge collection efficiency as a function of bias voltage for an irradiated device at a fluence $\phi = 10^{15}\mathrm{n_{eq}}/\mathrm{cm}^2$. The tracks are entering the detector either in the pixel region ("250 μm" from the trench) or in the un-instrumented region ("30", "40" and "50 μm" from the trench). The sensor has no GRs, and a 100 μm distance between edge and pixel.

after irradiation in that region, the edgeless concept would be verified to work. Our sensor was hit from the front side with simulated tracks created by a minimum ionizing particle (MIP) traversing 200 μm of silicon ($\sim$ 2.6 fC). The CCE was studied after a fluence of $\phi = 1 \times 10^{15}\mathrm{n_{eq}}/\mathrm{cm}^2$ as a function of the bias voltage for the detector with no GRs and a 100 μm trench-to-pixel distance. Four tracks impinging points have been considered: three in the edge region, at 30, 40 and 50 μm from the trench, and a fourth one in the pixel region, at a distance of 250 μm from the trench. In the following the different incidence points will be identified by their entry point distance from the trench. The charge collected by the pixel was defined as the integral over 100 ns[1] of the current flowing through the pixel, once the stable leakage current had been subtracted. Finally, the CCE was obtained by dividing this collected charge by the charge collected in the pixel region before irradiation [2]. In Figure 1 the CCE is presented as a function of the bias voltage for the simulated fluence for the four incidence points of the tracks.

At a fluence $\phi = 10^{15}\mathrm{n_{eq}}/\mathrm{cm}^2$, for a bias voltage of 300 V more than 50 % of the signal is collected in the region that is 30 μm away from the trench; as a comparison, 65 % of the signal is retained in the the pixel region. The expected collected charge in the region 30 μm away from the trench is then of ~8 ke [3], which corresponds to a signal large enough to trigger the FE-I4 readout chip.

---

[1] corresponding to 4 LHC bunch crossings

[2] This normalization was chosen since it correspnds to non-edge region for a non-irradiated bulk

[3] the MPV for the charge created by a MIP in 200 μm is 16 ke

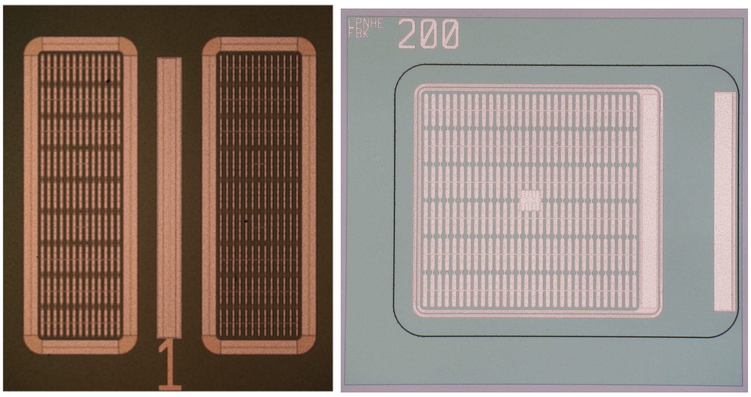

Figure 2. Left: test structures consisting of 2 arrays of 9 × 13 FE-I4-like pixel cells each (“interpixel structure”); the pixels in the left (right) structure have (no) field-plate. Right: test structures consisting of an array of 6 × 30 FE-I4-like pixel cells (“FE-I4 test structure”), where all the pixels were shorted together were used to evaluate the current voltage characteristics of the production.

4. Performance evaluation

Only one out of 20 processed wafers was not usable due to bad wafer-bonding. The electrical characterization of the production for non-irradiated sensors has been performed; it started with measurements on specially designed test structures, to assess mainly bulk and surface properties, then tests on large sensors followed. The first part of the measurement program was carried mainly on structures reported in Figure 2.

A test structure consisting of an array of 9 × 13 FE-I4-like pixel cells was used to measure the interpixel and the pixel-to-backside capacitance; the central pixel was isolated with respect to all the other pixels; the first 8 neighbours were shorted together, but isolated from all the other remaining (which, again, were shorted together). These structures are shown on the left in Figure 2, where two versions are present: one with metal field-plate and one without. “Interpixel structure” will be used for the sake of brevity in the remaining of the text to refer to this structure.

In Figure 2, on the right, an array of 6 × 30 FE-I4-like pixel cells is shown; all the pixels were shorted together allowing the measurement of the current voltage characteristics of the whole array and of the inner GR (if present), and the BD voltage dependence on the number of GRs and on the pixel-to-trench distance. Several combinations of values for the latter parameters are present on the wafer; in Figure 2, on the right, a structure with a 200 μm pixel-to-trench distance and 2 GRs is shown. “FE-I4 test structure” will be used for the sake of brevity in the remaining of the text to refer to this structure.

For the interpixel structure, in Figure 3 a) the inverse of the square capacitance between all the pixels and the sensor backside is presented as a function of the bias voltage; the measurement was performed at a frequency of 10 kHz. From this measurement the sensors’ depletion voltage was derived (∼20 V). For the same structure, in Figure 3 b) the capacitance between the central pixel and all the other ones is presented as a function of the bias voltage; the measurement has been carried out at three different frequencies: 10, 100 kHz and 1 MHz. It can be seen that the presence of a field-plate increases the interpixel capacitance. The coupling is particularly important due to

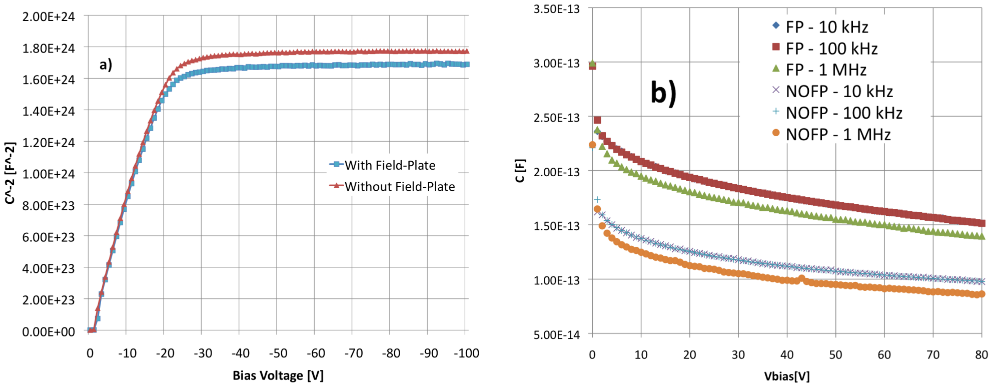

Figure 3. Measurements results for the intepixel structure; a) inverse squared capacitance between all the pixels and the sensor backside as a function of the bias voltage; both pixels with and without field-plate were tested; b) interpixel capacitance for test structure with FEI4-like cells; the capacitance between the central pixel and all the other pixels surrounding it in the test structure is reported as a function of the bias voltage for pixel cells with a field-plate, and without it; the results are reported for three different frequencies: 10, 100 kHz and 1 MHz.

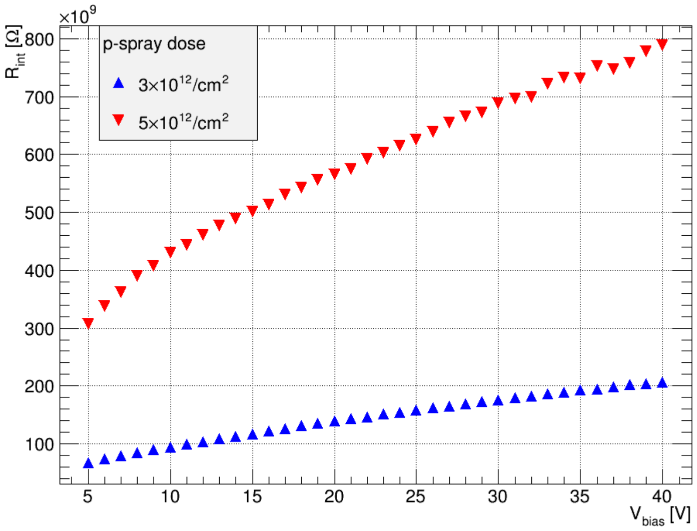

Figure 4. Interpixel capacitance as a function of the bias voltage for two different p-spray doses.

the presence of the uniform p-spray implant. However, the level of capacitative coupling, even with a field-plate, is acceptable in term of electronic noise for the read-out.

Using the interpixel structure the interpixel resistance was evaluated; the results are reported in Figure 4 for the 2 different p-spray doses. It can be seen that for the high p-spray dose value, at depletion voltage, the interpixel resistance is four times larger than the low p-spray dose corresponding value; nonetheless, excellent pixel isolation is already assured by low p-spray dose. After irradiation, this test will be crucial to prove the pixels isolation.

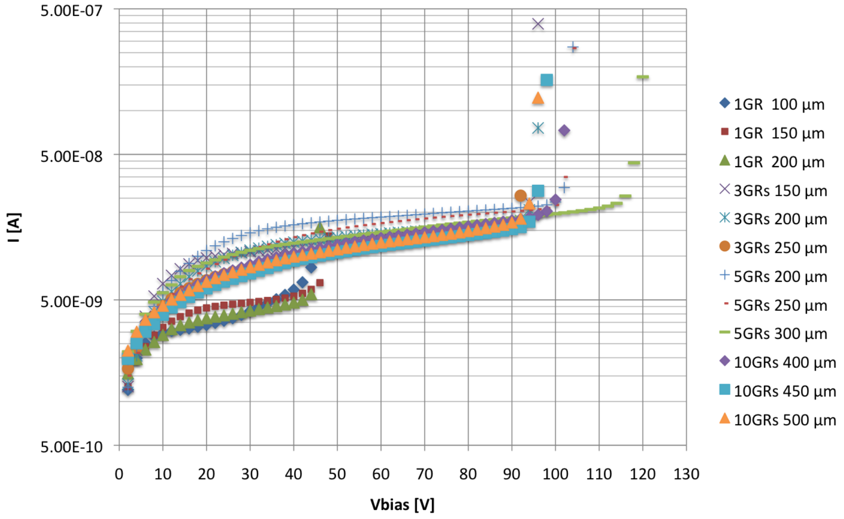

Figure 5. Current voltage characteristics for several FE-I4 test structures, differing by pixel-to-trench distance and by the number of GRs. The innermost GR was kept at ground (as well as the pixels) and the current flowing through is reported. Sensors were taken from a wafer featuring high p-spray dose.

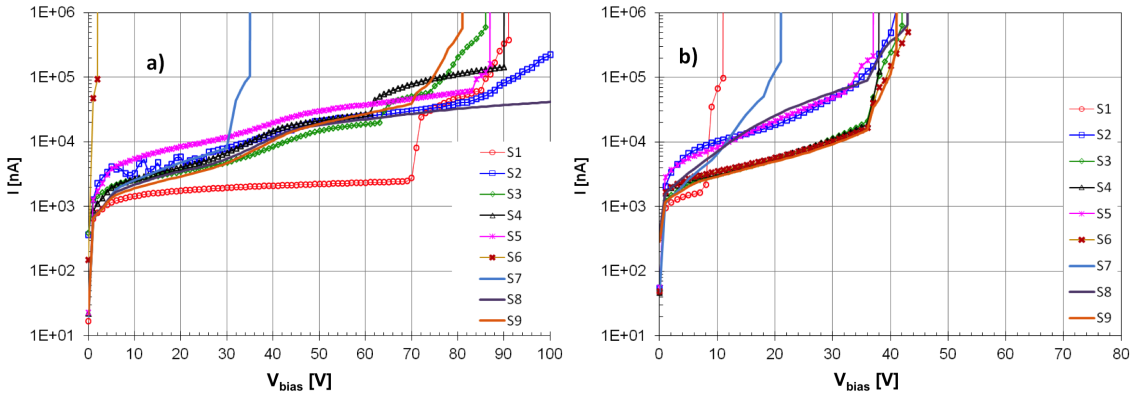

Figure 6. FE-I4 compatible sensors current voltage characteristics; a) p-spray dose on wafer was $3\times10^{12}/\text{cm}^2$; right: b) p-spray dose on wafer was $5\times10^{12}/\text{cm}^2$. Refer to text for the details on the different sensor layouts.

FE-I4 test structures were used to evaluate the current voltage characteristics of the production. The results are reported in Figure 5, for the sensors from a wafer featuring a high p-spray dose; the devices were reversely biased via the bias tab, the innermost GR was kept at ground (as well as the pixels), and the current flowing through the GR itself is reported.

As it can be seen, adding more GRs increase the BD voltage and a wider edge-to-pixel distance corresponds to more bulk generated-current. All sensors can be operated in over-depletion (the measured depletion voltage was of $\sim$20 V).

After having assessed the general production characteristics using the dedicated test structures, the FE-I4 compatible pixels sensors current voltage characteristics were measured. To this aim a temporary additional metal layer was used, as described in [9]. In Figure 6 the results are reported for two wafers, comparing sensors with two different p-spray implant doses; see Table 1 for the details on the different sensors' layouts. It can be seen that the higher the p-spray implant dose, the lower the BD voltage value; anyway, most of the sensors could be operated well in over-depletion. Large p-spray dose values are intended for after-irradiation operations, when larger oxide charges densities will make pixels isolation more challenging. These results are to be contrasted to the information contained in Figure 4: a large pixel dose assures an excellent pixel isolation, even after irradiation fluences comparable to those expected at the end of the HL-LHC phase, but they endanger operability due to low BD voltage. It must be said that anyway all but four defective sensors presented in Figure 6 can be operated in over-depletion and they are expected to show larger BD voltages after irradiation.

5. Conclusions and outlook

In view of the upgrade of the ATLAS Inner Detector for HL-LHC runs, FBK Trento and LPNHE Paris developed new planar n-on-p pixel sensors, characterized by a reduced inactive region at the edge thanks to a vertical doped lateral surface at the device boundary, the “active edge” technology. Simulation studies show the effectiveness of this technique in reducing the dead area, even after simulated fluences comparable to those expected at the end of the HL-LHC phase for the external layers. The measurements performed on real sensors, including capacitance- and current-voltage characteristics, show that it is possible to operate them successfully, well in over-depletion. Pixels isolation level is excellent even at low p-spray doses. Functional tests of the pixel sensors with radioactive sources, before and after irradiation, and eventually in a beam test, after having bump bonded a number of pixel sensors to the FE-I4 read out chips, will follow.

Acknowledgments

We acknowledge the support from the MEMS2 joint project of the Istituto Nazionale di Fisica Nucleare and Fondazione Bruno Kessler.

References

[1] L. Rossi and O. Brüning, *High Luminosity Large Hadron Collider A description for the European Strategy Preparatory Group*, CERN-ATS-2012-236, CERN, August 2012

[2] ATLAS TDR 19, CERN/LHCC 2010-013, *ATLAS Insertable B-Layer Technical Design Report*, `http://cdsweb.cern.ch/record/1291633/files/ATLAS-TDR-019.pdf`

[3] C. J. Kenney *et al.*, *Results from 3-D silicon sensors with wall electrodes: near-cell-edge sensitivity measurements as a preview of active-edge sensors*, IEEE Trans. Nucl. Sci. **NS-48 (6)** (2001) 2405.

[4] M. Bomben *et al.*, *Development of Edgeless n-on-p Planar Pixel Sensors for future ATLAS Upgrades* Nucl. Instr. and Meth. **A 712** (2013) 41 - 47.

[5] M. Garcia-Sciveres *et al.*, *The FE-I4 pixel readout integrated circuit*, Nucl. Instr. and Meth. **A 636** (2011) S155-S159.

[6] *Silvaco, Inc.*
4701 Patrick Henry Drive, Bldg 2
Santa Clara, CA 95054

[7] D. Pennicard *et al.*, *Simulations of radiation-damaged 3D detectors for the Super-LHC*, Nucl. Instr. and Meth. **A 592** (2008) 16-25.

[8] J. Schwandt *et al.*, *Optimization of the radiation hardness of silicon pixel sensors for high x-ray doses using TCAD simulations*, 2012 *JINST* **7** C01006

[9] G. Giacomini*et al.*, *Development of Double-Sided Full-Passing-Column 3D Sensors at FBK*, IEEE Transactions on Nuclear Science 60, (2013) 2357